Geophysical Journal International

Frequency response modeling of seismic waves using finite difference time domain with phase sensitive detection (TD-PSD)

Journal:	*Geophysical Journal International*
Manuscript ID:	GJI-05-0367.R2
Manuscript Type:	Research Paper
Date Submitted by the Author:	n/a
Complete List of Authors:	Nihei, Kurt; Chevron ETC, Seismic Analysis & Property Estimation Li, Xiaoye; Lawrence Berkeley National Laboratory, Computational Research Division
Keywords:	Finite-difference methods, Numerical techniques, Seismic modeling

Frequency response modeling of seismic waves using finite difference time domain with phase sensitive detection (TD-PSD)

Kurt T. Nihei[1] and Xiaoye Li[2]

[1]*Earth Sciences Division, Lawrence Berkeley National Laboratory; now at Chevron ETC, 6001 Bollinger Canyon Rd., San Ramon, CA 94583 USA. E-mail: knih@chevron.com*

[2]*Computational Research Division, Lawrence Berkeley National Laboratory, 1 Cyclotron Rd., MS 50F-1650, Berkeley, CA 94720 USA. E-mail: xsli@lbl.gov*

xxxxxxxxxxxxxxxxxxxx

SUMMARY

This paper describes an efficient approach for computing the frequency response of seismic waves propagating in 2D and 3D earth models within which the magnitude and phase are required at many locations. The approach consists of running an explicit finite difference time domain (TD) code with a time harmonic source out to steady state. The magnitudes and phases at locations in the model are computed using phase sensitive detection (PSD). Phase sensitive detection does not require storage of time series (unlike an FFT), reducing its memory requirements. Additionally, the response from multiple sources can be obtained from a single finite difference run by encoding each source with a different frequency. For 2D models with many sources, this time domain phase sensitive detection (TD-PSD) approach has a higher arithmetic complexity than direct solution of the finite difference frequency domain (FD) equations using nested dissection re-ordering (FD-ND). The storage requirements for 2D finite difference TD-PSD are lower than FD-ND. For 3D finite difference models, TD-PSD has significantly lower arithmetic complexity and storage requirements than FD-ND, and, therefore, may prove useful for computing the frequency response of large 3D earth models.

Key words: finite-difference methods, seismic modeling, numerical techniques.

1 INTRODUCTION

Computation of the frequency response (phase and magnitude) of seismic waves propagating in heterogeneous, anisotropic, viscoelastic media is required for a number of scientific and engineering endeavors, including frequency domain full-waveform inversion, earthquake site response modeling, and structural vibration studies. When the frequency response is required at a limited number of locations, it can be computed efficiently with a finite difference time domain (TD) code by storing the time series at specified receiver locations and computing the magnitude and phase with a fast Fourier transform (FFT). However, when the frequency response is required at many or all grid locations in the model, as in frequency domain full-waveform inversion (e.g., Pratt et al. 1998), the memory requirements for storing the waveforms at many model locations (for subsequent FFT analysis) make this approach prohibitive.

An alternative approach is to compute the frequency response by reformulating the finite difference equations in the frequency domain (FD) (Marfurt 1984; Štekl & Pratt 1998; Hustedt et al. 2004). The resulting linear system has the form $\boldsymbol{Ku}=\boldsymbol{f}$. For fourth order accuracy spatial differencing on a 2D elastic $n\times n$ finite difference grid, the system of implicit equations for $\boldsymbol{u}$ (the unknown particle velocities and stresses) at the finite difference cell locations is a large, complex, banded (band-diagonal with 8 sub-bands), sparse, non-Hermitian system matrix $\boldsymbol{K}$ with $O(n^2)$ non-zero entries. Direct solution of the 2D matrix using LU-factorization with nested dissection (ND) re-ordering requires $O(n^2 log_2 n)$ storage and $O(n^3)$ operations (arithmetic complexity), and, for an $n\times n\times n$ 3D problem, $O(n^4)$ storage and $O(n^6)$ operations (George & Liu 1981). An attractive feature of direct solution is its ability to provide solutions for additional sources $\boldsymbol{f}$ via a low cost backsubstitution. For typical 2D seismic exploration models (e.g., 10,000×2,500, $\boldsymbol{K}$ of $O(10^8)$) with several hundred sources, high performance sparse direct solution of the frequency domain system via nested dissection (FD-ND) (Li & Demmel 2003) is an efficient approach for computing of the entire-model frequency response. For large 3D problems, however, direct solution requires a prohibitive $O(n^6)$ operations. A viable alterative is to solve $\boldsymbol{Ku}=\boldsymbol{f}$ with an iterative method, recognizing that a separate iterative solution is now required for each source. For 3D problems, a simple

Krylov iterative solver without preconditioning and blocking requires $O(n^3)$ storage and a sparse matrix-vector multiplication requiring $O(n^3)$ operations per iteration. To speed up convergence, Krylov methods require a preconditioner (Barrett et al. 1994). For 2D acoustic wave propagation, Plessix & Mulder (2003) show that a separation-of-variables preconditioner and a bi-conjugate gradient (BICGSTAB) Krylov iterative solver yield acceptable convergence for smooth models and low frequencies. Unfortunately, poor convergence was observed as the frequency of the wave and the roughness of the model increase to values typically encountered in seismic exploration problems.

In the following sections, we examine an alternative approach for computing the frequency response of a heterogeneous, anisotropic, viscoelastic medium. The approach consists of running an explicit finite difference time domain (TD) code with a harmonic wave source out to steady-state, and then extracting the magnitude and phase from the transient data via phase sensitive detection (PSD). The PSD algorithm requires integration over a single cycle of the waveform to obtain accurate phase and magnitude estimates. Because this integration is performed by a summation over time, it is not necessary to store waveforms at all the grid locations, as would be required if a fast Fourier transform was employed. We also demonstrate that the response of multiple sources at different spatial locations can be obtained in a single finite difference run by encoding each source with a different frequency and extracting the phase and magnitude fields for each source (i.e., each frequency) via the PSD algorithm.

2 ENTIRE-MODEL FREQUENCY RESPONSE MODELING WITH FINITE DIFFERENCE TIME DOMAIN AND PHASE SENSITIVE DETECTION (TD-PSD)

In principle, the phase and magnitude fields can be computed from a finite difference time domain code by recording the time series at all locations in the model that are generated by a broadband source. For a 2D $n \times n$ model, this approach requires storage of n^2 time series of length N (i.e., $O(n^2 \cdot N)$ storage) and n^2 fast Fourier transforms (i.e., $O(n^2 \cdot N \log_2 N)$ operations; Press et al. 1992). For a 3D $n \times n \times n$ model, this

approach requires $O(n^3 \cdot N)$ storage and $O(n^3 \cdot N \log_2 N)$ operations. The large storage requirements make this approach intractable for large 2D and modest size 3D models.

2.1 Phase sensitive detection (PSD)

Here, we describe an alternative approach that can recover the magnitude and phase fields at a single frequency from finite difference time domain (TD) simulations performed with a time harmonic source. The approach, which is commonly employed in digital lock-in amplifiers to recover the magnitude and phase of very small AC signals with exceptionally high accuracy (e.g., Stanford Research Systems 1999), is referred to as *phase sensitive detection* (PSD). The PSD algorithm uses a reference waveform and a 90º phase shifted version of this reference waveform to compute the magnitude E_{sig} and phase θ_{sig} of the recorded signal ε_{sig}

$$\begin{aligned} \varepsilon_{sig} &= E_{sig}\cos(\omega t + \theta_{sig}) \quad \text{signal}, \\ \varepsilon_{ref\,0^\circ} &= E_{ref}\cos(\omega t + \theta_{ref}) \quad \text{reference (in-phase)}, \\ \varepsilon_{ref\,90^\circ} &= E_{ref}\cos(\omega t + \theta_{ref} + 90^\circ) \quad \text{reference (out-of-phase)}. \end{aligned} \tag{1}$$

The cross-correlation of the recorded signal ε_{sig} with the reference $\varepsilon_{ref\,0^o}$ over an integer number of periods mT gives the in-phase component of the signal X

$$X = \frac{1}{mT}\int_{t_S}^{t_S+mT}\left[\varepsilon_{sig}\cdot\varepsilon_{ref\,0^\circ}\right]dt\,. \tag{2}$$

The cross-correlation of the recorded signal ε_{sig} with the 90º phase shifted reference $\varepsilon_{ref\,90^o}$ over an integer number of periods mT gives the out-of-phase component of the signal Y

$$Y = \frac{1}{mT}\int_{t_S}^{t_S+mT}\left[\varepsilon_{sig}\cdot\varepsilon_{ref\,90^\circ}\right]dt\,. \tag{3}$$

The magnitude and phase of the signal are computed from the in-phase and out-of-phase components

$$\begin{aligned} \mathrm{E_{sig}} &= 2\sqrt{\mathrm{X}^2+\mathrm{Y}^2}\,\big/\,\mathrm{E_{ref}} \\ \theta_{\mathrm{sig}} &= \tan^{-1}(\mathrm{Y}/\mathrm{X}) + \theta_{\mathrm{ref}}\,, \end{aligned} \tag{4}$$

which can be verified by substitution of eqs (1)-(3) into eq. (4).

Practical implementation of the PSD approach in a finite difference TD code requires two pieces of information: (1) a starting time t_S at which the integration should commence, and (2) the number of periods mT required for an accurate estimate of the magnitude and phase. For the former, a simple criterion based on the travel time of the slowest shear waves in the model is used (Appendix A). For the latter, experience with the TD-PSD approach has demonstrated that a single period (i.e., $m=1$) of integration is sufficient to obtain accurate phase and magnitude estimates.

Because the PSD approach requires a simple integration over time, the magnitude and phase computations do not require the storage of time series. This significantly reduces the storage requirements over the fast Fourier transform approach in applications that require the computation of the magnitude and phase at many locations in the finite difference model, such as frequency domain full-waveform inversion (Pratt et al. 1998; Sirgue & Pratt 2004). It should be noted that, taken collectively, the PSD eqs (1)-(3) have the form of a discrete Fourier transform (DFT) for the specific case where the signal is a harmonic wave, the reference wave has a magnitude of 1 and a phase of zero (i.e., $E_{ref} = 1$ and $\theta_{ref} = 0$), and the integration is over integer multiples of the wave period T. The application of a DFT, which like PSD, is also a running sum over time calculation, to extract the frequency response of finite difference time domain electromagnetic wave propagation simulations is described by Furse (2000).

2.2 Accuracy test

The accuracy of the TD-PSD approach for computing the phase and magnitude fields is established for a 2D isotropic elastic inclusion model through a comparison with a frequency domain boundary element method (BEM) solution (Nihei 2005). Because the BEM solution is constructed from the analytic Green's function for elastic waves, experience has shown that it can be very accurate when the numerical integration is performed at ~8-10 points per shear wavelength. However, the computational expense of forming and solving the implicit system of complex, non-sparse BEM equations limits its applicability to simplistic earth models.

For the BEM–finite difference TD-PSD comparison, the model consists of a square region containing higher P- and S-wave velocities (Fig. 1). A vertical body force source driven at 30 Hz excites both P- and S-waves that superimpose in space and time to form simple harmonic particle motion at every point in the model (Fig. 1).

The finite difference TD modeling was carried out using an elastic staggered grid code with $O(2)$ time and $O(4)$ space differencing accuracies (Levander 1988). The magnitude and phase fields are computed via the PSD approach (i.e., eqs (1)–(4)). The integrations in eqs (2) and (3) are started at t_S = 0.4 s. A comparison of the recorded particle velocity at a location x = 200 m, z = -600 m and that reconstructed from the PSD computed magnitude and phase is displayed in Fig. 2. At this particular receiver location, simple harmonic motion (i.e., a steady-state) is achieved by 0.4 s. Accurate PSD estimates of the particle velocity are evident at integer multiples of the wave period T = 1/(30 Hz), where the autocorrelations in eqs (2) and (3) "lock-in" to the correct magnitude and phase.

A comparison of the BEM and finite difference TD-PSD computed magnitude and phase fields are shown in Fig. 3 for the vertical particle velocity. The finite difference TD-PSD computed magnitude and phase fields show very good agreement in the region interior to the absorbing boundaries (indicated by the dashed box).

Detailed comparisons of the magnitude and phase along the profile at z = -500 m are displayed in Fig. 4. The agreement between the BEM and finite difference TD-PSD magnitudes and phases is very good in the region interior to the absorbing boundaries of the finite difference model.

2.3 SEG/EAGE salt model example

The subsurface can exhibit a range of complexities for elastic waves, including multi-scale heterogeneities, anisotropy, and attenuation. To be of practical value, the TD-PSD approach must be capable of computing the frequency response in earth models with realistic complexity. In this section, TD-PSD is used to extract the frequency response of elastic waves propagating in the 2D SEG/EAGE salt model (Aminzadeh et al. 1994).

The 2D SEG/EAGE salt model contains a high velocity salt body embedded in faulted and variable thickness sediments typical of the Gulf of Mexico (Fig. 5). The model is isotropic with a constant density (2450 kg/m^3) and a constant Poisson's ratio (ν = 0.25). The 16.2×3.7 km finite difference model was discretized into 12.2×12.2 m cells to form a 1324×300 mesh. A stress-free boundary condition was set at the top of the model to represent the surface of the ocean. A 30 Hz cosine wave (tapered on its leading edge) was injected 3.7 m below the ocean surface at location x = 3.7 km. The finite difference simulations on this model were carried out to 41 s with a time step of 1.5 ms using an O(2,4) viscoelastic staggered grid finite difference TD code (Robertsson et al. 1994).

Traces for a receiver located in the bottom right-hand corner of the model (x = 15.1 km, z = 3.1 km) are displayed in Fig. 6 for two values of attenuation: $Q = \infty$ (zero attenuation) and Q = 150 (considered near the upper bound of Q values for Gulf of Mexico sediments). This result demonstrates the long times required to achieve steady-state (i.e., simple harmonic motion) in a purely elastic model. In fact, the traces in Fig. 6 show that a steady-state condition is not achieved in the 41 s simulation time for the $Q = \infty$ model, while it is achieved at ~15 s in the Q = 150 model. Thus, incorporating realistic Q values in the model can significantly reduce the number of time steps required to achieve steady-state conditions.

The magnitude and phase of the vertical particle velocity were computed at every cell in the finite difference model, and are displayed in Fig. 7 for the two Q values. As expected, attenuation has a strong effect on the spatial decay of the magnitude away from the source, while the corresponding phase changes are more subtle.

3 MULTI-SOURCE MODELING USING TD-PSD WITH FREQUENCY-ENCODED SOURCES

Frequency response measurements by a lock-in detector are made possible by the PSD's ability to accurately isolate the frequency response at the specified frequency while rejecting contributions from other frequencies (Stanford Research Systems 1999). This feature can be exploited in finite difference TD-PSD modeling to compute the frequency response at multiple frequencies from a single run by superimposing multiple frequencies at the source or to compute the frequency response for multiple

sources by encoding each with a slightly different frequency. Multi-frequency PSD is described in further detail below.

3.1 Multi-frequency PSD

When multiple frequencies are present in the signal, beating (modulation) will occur (Kinsler et al. 1982), thereby altering the condition required to obtain stable estimates of the magnitudes and phases using PSD. For the case of a source emitting two frequencies, the following analysis will show that stable estimates of the magnitude and phase can be obtained by integrating over the inverse of a beating frequency defined by the difference of the two frequencies.

To demonstrate this, consider the case of two cosine waves with different frequencies ω_1 and ω_2 being injected into a medium (either two separate sources, or a single source emitting the superposition of two cosine waves),

$$\begin{aligned} \varepsilon_{sig} &= E_{sig\,1}\cos(\omega_1 t + \theta_{sig\,1}) + E_{sig\,2}\cos(\omega_2 t + \theta_{sig\,2}) \quad \text{signal} \\ \varepsilon_{ref\,1(0^\circ)} &= E_{ref\,1}\cos(\omega_1 t + \theta_{ref\,1}) \quad \text{reference (in-phase for } \omega_1) \\ \varepsilon_{ref\,1(90^\circ)} &= E_{ref\,1}\cos(\omega_1 t + \theta_{ref\,1} + 90^\circ) \quad \text{reference (out-of-phase for } \omega_1)\ . \end{aligned} \tag{5}$$

Following eq. (2), form the in-phase component for frequency ω_1 by cross-correlation with the reference,

$$\begin{aligned} X_1 &= \frac{1}{T_B}\int_0^{T_B}\left[\varepsilon_{sig}\cdot\varepsilon_{ref\,1(0^\circ)}\right]dt \\ &= \frac{E_{sig\,1}E_{ref\,1(0^\circ)}}{2T_B}\int_0^{T_B}\left[\cos(\theta_{sig\,1}-\theta_{ref\,1(0^\circ)}) + \cos(2\omega_1 t + \theta_{sig\,1} + \theta_{ref\,1(0^\circ)})\right]dt \\ &+ \frac{E_{sig\,2}E_{ref\,1(0^\circ)}}{2T_B}\int_0^{T_B}\left\{\cos\left[\Delta\omega_B t + \theta_{sig\,2} - \theta_{ref\,1(0^\circ)}\right] + \cos\left[(\omega_1+\Delta\omega_B)t + \theta_{sig\,2} - \theta_{ref\,1(0^\circ)}\right]\right\}dt\ , \end{aligned} \tag{6}$$

where $\Delta\omega_B = (\omega_2 - \omega_1)$, and for simplicity the limits of the integral are relative to the simulation time at which steady-state conditions are achieved (t_s in eqs (2) and (3)). If the integration time is selected with the following properties,

$$T_B = \frac{2\pi}{\Delta\omega_B}$$
$$\omega_2 = \omega_1 + n\Delta\omega_B, \text{ where } n \geq 1 \text{ is an integer} , \tag{7}$$

then the contribution of signal ω_2 (second integral) drops out, and the in-phase contribution of signal ω_1 is recovered,

$$\begin{aligned} X_1 &= \frac{\Delta\omega_B E_{sig1} E_{ref1(0^\circ)}}{4\pi} \int_0^{\frac{2\pi}{\Delta\omega_B}} \left[\cos(\theta_{sig1} - \theta_{ref1(0^\circ)}) + \cos(4\pi n\Delta\omega_B t + \theta_{sig1} + \theta_{ref1(0^\circ)}) \right] dt \\ &+ \frac{\Delta\omega_B E_{sig2} E_{ref1(0^\circ)}}{4\pi} \int_0^{\frac{2\pi}{\Delta\omega_B}} \left\{ \cos\left[\Delta\omega_B t + \theta_{sig2} - \theta_{ref1(0^\circ)} \right] + \cos\left[(n+1)\Delta\omega_B t + \theta_{sig2} - \theta_{ref1(0^\circ)} \right] \right\} dt \\ &= \frac{E_{sig1} E_{ref1(0^\circ)}}{2} \cos(\theta_{sig1} - \theta_{ref1(0^\circ)}) . \end{aligned} \tag{8}$$

Following the same procedure for the out-of-phase component gives,

$$\begin{aligned} Y_1 &= \frac{1}{T_B} \int_0^{T_B} \left[\varepsilon_{sig1} \cdot \varepsilon_{ref1(90^\circ)} \right] dt \\ &= \frac{\Delta\omega_B E_{sig1} E_{ref1(0^\circ)}}{4\pi} \int_0^{\frac{2\pi}{\Delta\omega_B}} \left[\sin(\theta_{sig1} - \theta_{ref1(90^\circ)}) - \sin(4\pi n\Delta\omega_B t + \theta_{sig1} + \theta_{ref1(90^\circ)}) \right] dt \\ &+ \frac{\Delta\omega_B E_{sig2} E_{ref1(0^\circ)}}{4\pi} \int_0^{\frac{2\pi}{\Delta\omega_B}} \left\{ \sin\left[\Delta\omega_B t + \theta_{sig2} - \theta_{ref1(0^\circ)} \right] + \sin\left[(n+1)\Delta\omega_B t + \theta_{sig2} - \theta_{ref1(0^\circ)} \right] \right\} dt \\ &= \frac{E_{sig1} E_{ref1(90^\circ)}}{2} \sin(\theta_{sig1} - \theta_{ref1(90^\circ)}) . \end{aligned} \tag{9}$$

Application of eq. (4) to eqs (8) and (9) gives the estimates of the magnitude and phase for the ω_1 component of the signal. The same analysis can be applied to extract the ω_2 component of the signal. This result demonstrates that recovery of the magnitude and phase for a signal composed of two harmonic waves with different frequencies is possible if the integration time is set to the beating period $T_B = 2\pi/\Delta\omega_B$.

This analysis can be generalized to the case of $N_f > 2$ frequencies to show that multi-frequency PSD is possible for a signal composed of many frequencies provided that a constant frequency separation $\Delta\omega_B$ is maintained between the frequencies. As with the two frequency example given above, the

constant frequency separation for the $N_f > 2$ case allows the PSD integration over $T_B = 2\pi/\Delta\omega_B$ to accurately recover the magnitudes and phases for each frequency component contained in the signal.

3.2 Frequency-encoded sources

Recent work on finite difference frequency domain migration and full-waveform inversion (Mulder & Plessix 2004; Sirgue & Pratt 2004) demonstrate that subsurface imaging of structure and properties is possible with far-fewer frequencies ($N_f < 10$) than prescribed by Nyquist theorem. This work has also demonstrated that a scale approach to frequency domain inversion in which the inversion is progressed from low frequency to high better ensures convergence to the global solution. Because seismic reflection surveys can have hundreds (2D) to thousands (3D) of spatially-distributed sources and in order to preserve the scale approach, it is desirable to have a frequency response seismic modeling engine that can efficiently model many sources around a narrow frequency band.

The multi-frequency PSD described in 3.1 offers the possibility of obtaining the frequency response from many sources in a single finite difference TD simulation by encoding each source with a different frequency. As discussed in the previous section, for more than two frequencies, each frequency should be separated by a constant Δf_B in order for the PSD integration to accurately recover the magnitude and phase.

Fig. 8 shows the layout for three frequency-encoded sources propagating in the SEG/EAGE salt model (Q = 150). In this model, the sources have frequencies $f = 30\,\text{Hz} + n\Delta f_B$, where $n = 0,1,2$ and $\Delta f_B = 0.1\,\text{Hz}$. Fig. 9 shows the trace recorded at the receiver located in the bottom right corner of the model (Fig. 8). Comparison of Fig. 9 with the trace from the single source simulation (Fig. 6) shows the $T_B = 1/\Delta f_B = 10\,\text{s}$ beating resulting from the superposition of the three frequencies. The magnitude and phase of the vertical particle velocity were computed at every grid location in the finite difference model. These values were then used to reconstruct a snapshot of the time-harmonic wavefield (Fig. 10) using eq.

(1). Clear separation of the wavefields for each source can be seen, indicating that the PSD is capable of extracting the wavefield from each source, with negligible contributions from the other sources.

4 ANALYSIS OF THE COMPUTATIONAL REQUIREMENTS FOR 2D AND 3D FINITE DIFFERENCE TD-PSD

In this section, we provide estimates of the storage and number of operations (arithmetic complexity) for multi-source frequency response modeling using 2D ($n \times n$) and 3D ($n \times n \times n$) finite difference TD-PSD. We focus our motivation here on the scale approach to frequency domain full-waveform inversion (discussed at the beginning of section 3.2) in which the solution strategy is to carry out the inversion for many (spatially-distributed) sources, starting at a low frequency and progressing to higher frequencies (Mulder & Plessix 2004; Sirgue & Pratt 2004). For this strategy, the TD-PSD approach can be applied in two flavors: (1) TD-PSD$_{SS}$ consisting of N_S individual single source runs, with all runs at the same frequency, and (2) TD-PSD$_{FES}$ consisting of a single run with N_S frequency-encoded sources. In the second approach, the frequency spacing between the frequency encoded sources, Δf_B, is selected such that $N_S \cdot \Delta f_B$ is small (i.e., narrow bandwidth).

The operation count for a 3D ($n \times n \times n$) finite difference model using the first approach (TD-PSD$_{SS}$) is

$$OC_{(1)} = N_S \left[N_t \cdot n^3 \cdot A + N_T \cdot n^3 (A + B) \right] \approx N_S \cdot N_t \cdot n^3 \cdot A \quad , \quad for\ N_t \gg N_T \quad , \tag{10}$$

where

$N_S \equiv$ number of sources
$N_t \equiv$ number of time steps to reach steady state
$N_T \equiv$ number of time samples in one period of the propagating wave
$A \equiv$ number of operations in the finite difference TD algorithm
$B \equiv$ number of operations in the PSD algorithm.

The operation count for a 3D ($n \times n \times n$) finite difference model using the second approach (TD-PSD$_{FES}$) is

$$OC_{(2)} = N_t \cdot n^3 \cdot A + N_{T_B} \cdot n^3 (A + N_S \cdot B)$$
$$= N_t \cdot n^3 \cdot A \left\{ 1 + \frac{N_{T_B}}{N_t} \left[1 + N_S \left(\frac{B}{A} \right) \right] \right\} \quad , \tag{11}$$

where $N_{T_B} = T_B / \Delta t$ is the number of time steps in one beat cycle.

The ratio between eqs (10) and (11) has the form

$$R = \frac{OC_{(1)}}{OC_{(2)}} \approx \frac{N_S}{1 + \frac{N_{T_B}}{N_t} \left[1 + N_S \left(\frac{B}{A} \right) \right]}$$
$$\approx \frac{N_S}{1 + \frac{1}{\Delta f_B \Delta t \, N_t} \left[1 + N_S \left(\frac{B}{A} \right) \right]} \quad . \tag{12}$$

When eq. (12) is plotted as a function of the number of sources N_S and the product $N_S \Delta f_B$ (i.e., the frequency bandwidth occupied by the N_S sources each separated by Δf_B), a trade-off curve results (Fig. 11). This curve illustrates that if it is desirable to keep the frequency spread between the first and last source in the simulation to a minimum (i.e., a small value of $N_S \Delta f_B$), as in the strategy for frequency domain full-waveform inversion discussed at the beginning of section 3.2, then there is an optimum number of sources that can be used in TD-PSD$_{\text{FES}}$ to achieve the maximum speed-up over TD-PSD$_{\text{SS}}$. For an assumed ratio of $(B/A) = 1/10$ and an upper bound of $N_S \Delta f_B = 5$ Hz, the TD-PSD$_{\text{FES}}$ speed-up is ~10× when 15-40 sources are used. Because the model size has dropped out of the ratio eq. (12), this result also holds for 2D TD-PSD$_{\text{FES}}$.

Table 1 gives the computational efficiency (big-*O*) estimates for both flavors of TD-PSD for the multiple source problem. Note that these order of magnitude estimates do not reflect the smaller gains described in eq. (12), i.e., both flavors of TD-PSD have the same operation counts. Also note that for problems with many sources, TD-PSD$_{\text{FES}}$ requires N_S more storage for the additional magnitude and phase fields for each source.

Also shown in Table 1 for reference are the estimates of storage and number of operations for direct solution of the finite difference frequency domain equations by LU-factorization with the nested dissection reordering method (FD-ND; George & Liu 1981). For 2D problems with many sources, FD-ND is an effective solution strategy: both TD-PSD$_{SS}$ and TD-PSD$_{FES}$ require a factor N_S more operations than FD-ND, but TD-PSD$_{SS}$ has lower storage requirements. For 3D problems, both TD-PSD approaches have significantly lower number of operations than FD-ND. TD-PSD$_{SS}$ is superior to both TD-PSD$_{FES}$ and FD-ND in storage requirements.

The storage and operation count estimates in Table 1 suggest that for most 2D frequency response modeling problems (many sources, ample memory), FD-ND is the method of choice. For large, memory-limited 3D problems (e.g., 10,000×2,500×2,500) typical in seismic exploration, multi-source frequency response modeling is best addressed with TD-PSD$_{SS}$, i.e., by running N_S single source TD-PSD runs.

5 SUMMARY

This paper presents an approach for computing the frequency response of realistic earth models using an explicit finite difference time domain (TD) code and a phase sensitive detection (PSD) algorithm. In the TD-PSD approach, the frequency response of seismic waves is computed by running the finite difference TD code with a harmonic wave source out to steady-state, and then extracting the magnitude and phase from the transient data via a cross-correlation with in-phase and out-of-phase reference cosine waves. The PSD algorithm requires integration over a single cycle of the waveform to obtain accurate phase and magnitude estimates. Because this integration is performed by a running summation over time, it is not necessary to store waveforms at the grid locations, as would be the case if an FFT was used. Comparisons of the finite difference TD-PSD approach with a frequency domain boundary element method (BEM) solution demonstrate the accuracy of this approach. Simulations in the SEG/EAGE salt model demonstrate the importance of including (realistic) attenuation in the model to reduce the time

required to achieve steady state conditions (simple harmonic motion). It was demonstrated that the TD-PSD approach can be used to obtain the frequency response of multiple sources in a single finite difference TD run by encoding each source with a different frequency (TD-PSD$_{FES}$). The presence of multiple sources gives rise to beating, and analysis of the multi-frequency PSD demonstrates that the PSD integration must be made over the beat period of the interfering waves to accurately recover the magnitude and phase.

Analysis of the operation counts suggests that significant speed-ups can be achieved with the frequency-encoded source approach TD-PSD$_{FES}$ relative to the more conventional TD-PSD$_{SS}$ approach where separate single source runs are performed. Analysis of the storage for TD-PSD$_{FES}$, however, indicates that this approach requires significantly more memory to store the magnitude and phase fields for all the sources. For large 3D problems, this additional storage may render the TD-PSD$_{FES}$ approach intractable. The analysis shows that the straightforward TD-PSD$_{SS}$ approach of running separate finite difference models for each source is the best approach for 3D frequency response modeling, with significantly lower storage and operations than a direct solution of the finite difference frequency domain equations using nested dissection re-ordering (FD-ND). Further work is required to examine the performance of TD-PSD in realistic 3D earth models, and to investigate potential avenues for increasing its computation efficiency.

ACKNOWLEDGMENTS

This work was supported by the Director, Office of Science, Office of Basic Energy Sciences, Division of Chemical Sciences, Geosciences, and Biosciences of the U.S. Department of Energy under Contract No. DE-AC03-76SF00098. We thank Jonathan Ajo-Franklin, Valeri Korneev, and Joe Stefani for insightful discussions on monochromatic waves, and the reviewers for improving the content and readability of the paper.

REFERENCES

Aminzadeh, F., Burkhard, N., Nicoletis, L., Rocca, F. & Wyatt, K., 1994. SEG/EAGE 3-D modeling project: 2nd update, *The Leading Edge*, **13**, 949-952.

Barrett, R., Michael, B., Chan, T.F., Demmel, J., Donato, J., Dongarra, J., Eijkhout, V., Pozo, R., Romine, C. & van der Vorst, H., 1994. *Templates for the Solution of Linear Systems: Building Blocks for Iterative Methods*, SIAM, Philadelphia.

Furse, C.M., 2000. Faster than Fourier-ultra-efficient time-to-frequency domain conversions for FDTD simulations, *Antennas & Propagation Mag.*, **42**, 24-34.

George, J.A. & Liu, J.W.H., 1981. *Computer Solution of Large Sparse Positive Definite Systems*, Prentice-Hall, New Jersey.

Hustedt, B., Operto, S. & Virieux, J., 2004. Mixed-grid and staggered-grid finite-difference methods for frequency-domain acoustic wave modelling, *Geophys. J. Int.*, **157**, 1269-1296.

Kinsler, L.E., Frey, A.R., Coppens, A.B. & Sanders, J.V., 1982. *Fundamentals of Acoustics*, 3rd edn, pp. 20-23, John Wiley & Sons, New York.

Levander, A.R., 1988. Fourth-order finite-difference *P-SV* seismograms, *Geophysics*, **53**, 1425-1436.

Li, X.S. & Demmel, J., 2003. SuperLU_DIST: A scalable distributed-memory sparse direct solver for unsymmetric linear systems, *ACM Trans. on Mathematical Software*, **29**, 110-140. http://crd.lbl.gov/~xiaoye/SuperLU/

Marfurt, K.J., 1984, Accuracy of finite difference and finite element modeling of the scalar and elastic wave equations, *Geophysics,* **49**, 533-549.

Mulder, W.A. & Plessix, R.-E., 2004. How to choose a subset of frequencies in frequency-domain finite-difference migration, *Geophys. J. Int.*, **158**, 801-812.

Nihei, K.T., 2005. *BE2D: A 2D Boundary Element Code for Computing the Frequency Response of Elastic Waves in Heterogeneous Media with Imperfect Interfaces*, Lawrence Berkeley National Laboratory Report, **LBNL-58685**, Berkeley.

Plessix, R.E. & Mulder, W.A., 2003. Separation-of-variables as a preconditioner for an iterative Helmholtz solver, *Applied Numerical Mathematics,* **44**, 385-400.

Pratt, R.G., Shin, C. & Hicks, G.J., 1998. Gauss-Newton and full Newton methods in frequency space seismic waveform inversion, *Geophys. J. Int.,* **133**, 341-362.

Press, W.H., Teukolsky, S.A., Vetterling, W.T. & Flannery, B.P., 1992. *Numerical Recipes in C,* 2nd edn, pp. 504, Cambridge University Press, Cambridge.

Robertsson, J.O.A, Blanch, J.O. & Symes, W.W., 1994. Viscoelastic finite-difference modeling, *Geophysics.*, **59**, 1444-1456.

Sirgue, L. & Pratt, R.G., 2004. Efficient waveform inversion and imaging: A strategy for selecting temporal frequencies, *Geophysics*, **69**, 231-248.

Stanford Research Systems, 1999. DSP Lock-In Amplifier Model 850, Rev. 1.4. http://www.thinksrs.com/downloads/PDFs/Manuals/SR830m.pdf

Štekl, I. & Pratt, R.G., 1998. Accurate viscoelastic modeling by frequency-domain finite differences using rotated operators, *Geophysics*, **63**, 1779-1794.

APPENDIX A: Demonstration that $N_t \sim O(n)$

Let the number of time steps that a 2D ($n \times n$) or 3D ($n \times n \times n$) finite difference TD code must be run to in order to attain steady-state wavefields (i.e., simple harmonic motion) be defined as

$$N_t = \frac{t_S}{\Delta t} \ . \qquad \text{(A1)}$$

In eq. (A1), t_S is selected large enough to include the slowest arrivals coming from the most distant parts of the model. As a conservative estimate, we take this to be the travel time it takes a shear wave to propagate across five lengths $5L$ of the largest model dimension at the slowest shear velocity c_{Smin} contained in the model

$$t_S = \frac{5L}{c_{S\min}} = \frac{5n\Delta l}{c_{S\min}} \ , \tag{A2}$$

where Δl is the grid size. We will see at the end of this analysis that doubling or tripling this distance estimate will not alter the final result. The time step Δt is prescribed by the stability condition for a fourth order spatial differencing scheme (Levander 1988)

$$\Delta t \le \frac{\Delta l}{\sqrt{2}\, c_{P\max} \sum_{i=0,1} |c_i|} = 0.6061\, \Delta l / c_{P\max} \ , \tag{A3}$$

where c_0= 9/8 and c_1= -1/24 are the inner and outer coefficients of the fourth order approximation to the first derivative.

Substituting eqs (A2) and (A3) into eq. (A1) gives

$$N_t = \frac{5n}{0.6061(c_{S\min}/c_{P\max})} \sim O(n) \ . \tag{A4}$$

Because "big-O" notation operation estimates are essentially proportionality estimates for large inputs (i.e., large n), it is clear that the relation (A4) still holds even if we had used a larger estimate of the maximum propagation path.

FIGURE LEGENDS (11)

Figure 1. Snapshots of the vertical particle velocity taken at $\omega t = \pi$: (left) BEM, and (right) reconstructed from the TD-PSD computed magnitudes and phases. The model consists of a higher velocity 200×200 m square inclusion (V_P = 4000 m/s, V_S = 2406 m/s, ρ = 2200 kg/m^3) embedded in an infinite space (V_P = 3300 m/s, V_S = 1700 m/s, ρ = 2350 kg/m^3). The source is a vertical body force driven at 30 Hz. The results show very close agreement except in the outer 150 m of the finite difference time domain model (region outside the dashed lines) where absorbing boundaries are applied.

Figure 2. Finite difference time domain particle velocity (vertical component) at a location x = 200 m, z = -600 m: (solid) recorded, and (dotted) reconstructed from the TD-PSD computed magnitude and phase. The arrows indicate integral multiples of the wave period T where the PSD integration "locks-in" to the correct particle velocity magnitude and phase.

Figure 3. Comparison of the magnitude and phase fields of the vertical particle velocity computed by: (left column) BEM, and (right column) TD-PSD. The magnitude fields are displayed in the upper row, and the phase fields in the lower row. The dashed box in the TD-PSD figures indicates the location of the absorbing boundaries. The solid horizontal line is the profile along which the fields are compared in Fig. 4.

Figure 4. Detailed comparison of the magnitude and phase of the vertical particle velocity along the profile z= -500 m computed by: (solid line) BEM, and (circles) TD-PSD. The vertical dashed lines show the location of the absorbing boundaries in the finite difference model, and the vertical solid lines show the location of the high velocity inclusion.

Figure 5. SEG/EAGE salt model used to test the finite difference TD-PSD approach for estimating the frequency response. A 30 Hz source is located near the free-surface, and a monitor receiver is embedded in the bottom-right corner of the model.

Figure 6. The traces recorded at the monitor receiver (Fig. 5). Note that the effect of adding attenuation to the model (Q = 150) is to significantly reduce the time at which steady-state (simple harmonic motion) is achieved.

Figure 7. The magnitude (a) and phase (b) fields of the vertical particle velocity computed with finite difference TD-PSD for two Q values.

Figure 8. SEG/EAGE salt model with the locations of the three sources used in the multi-source test of TD-PSD$_{FES}$. The source frequencies used were 30.0, 30.1, and 30.2 Hz.

Figure 9. The trace recorded at the monitor receiver for the frequency-encoded three source example (Fig. 8). The frequency difference between each of the three sources, $\Delta f = 0.1$ Hz , gives rise to beating with a period of 10 s.

Figure 10. Vertical particle velocity transient fields at 40 s constructed for each of the three sources from the TD-PSD$_{FES}$ computed magnitudes and phases. The computed wavefields show a clean separation of wave motion coming from each source.

Figure 11. Trade-off plot of the speed-up that can be obtained for multiple source frequency response modeling using frequency encoded sources (TD-PSD$_{FES}$) relative to the more conventional approach in which each source is modeled in a separate finite difference run (TD-PSD$_{SS}$). The trade-off is between

the number of frequency-encoded sources and the frequency spread (between the first and last source) that can be tolerated. The boxed region highlights the range of speed-ups possible with TD-PSD$_{FES}$ for 15-40 sources and a frequency bandwidth of 1-5 Hz.

TABLES (1)

Table 1. Storage and operation requirements for 2D ($n \times n$) and 3D ($n \times n \times n$) multiple source finite difference frequency response modeling: FD-ND denotes frequency domain (FD) solution via nested dissection (ND) re-ordering, and TD-PSD denotes time domain (TD) solution via phase sensitive detection (PSD). N_S is the number of sources, N_t is the number of time steps required to attain a steady state wavefield (see Appendix A), and N_{T_B} is the number of time steps in one beat period.

Finite Difference Frequency Response Modeling	FD-ND	TD-PSD$_{SS}$ N_S single source runs	TD-PSD$_{FES}$ single run with N_S frequency-encoded sources
2D Storage	$O(n^2 \log_2 n)$	$O(n^2)$	$O(n^2 \cdot N_S)$
2D #Operations	$O(n^3)$	$O(n^2 \cdot N_t \cdot N_S)$ $\sim O(n^3 \cdot N_S)$	$O(n^2 \cdot N_{T_B} \cdot N_S)$ $\sim O(n^3 \cdot N_S)$
3D Storage	$O(n^4)$	$O(n^3)$	$O(n^3 \cdot N_S)$
3D #Operations	$O(n^6)$	$O(n^3 \cdot N_t \cdot N_S)$ $\sim O(n^4 \cdot N_S)$	$O(n^3 \cdot N_{T_B} \cdot N_S)$ $\sim O(n^4 \cdot N_S)$

FIGURES (11)

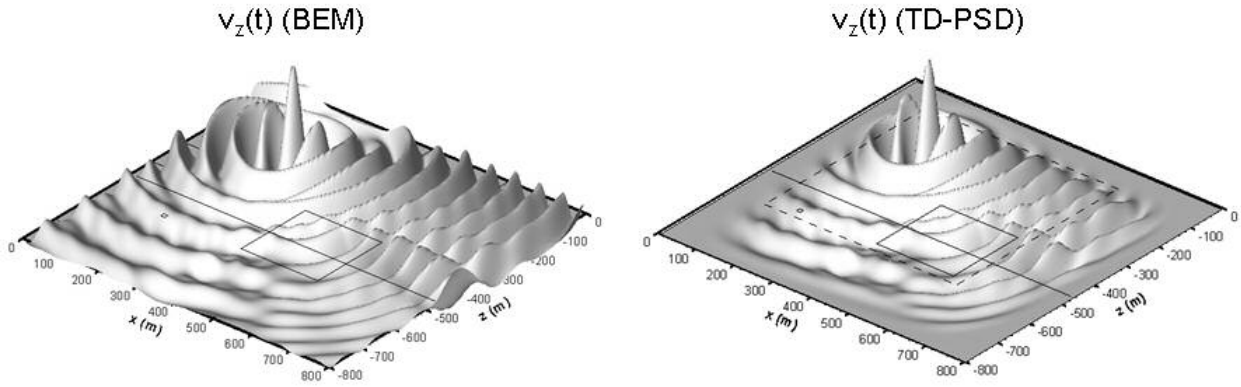

Figure 1

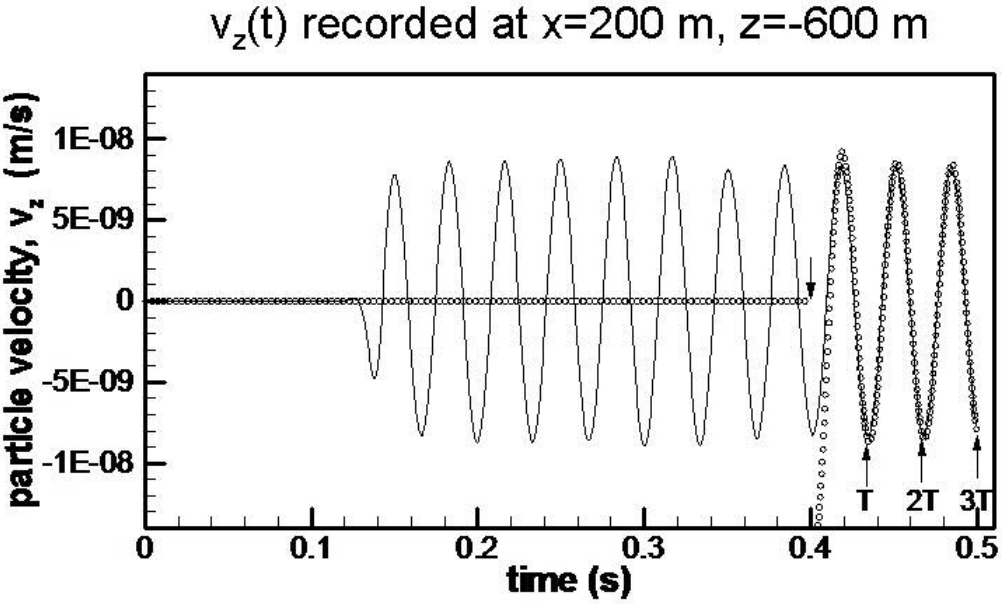
v_z(t) recorded at x=200 m, z=-600 m
particle velocity, v_z (m/s)
1E-08
5E-09
0
-5E-09
-1E-08
0
0.1
0.2
0.3
0.4
0.5
time (s)
T
2T
3T

Figure 2

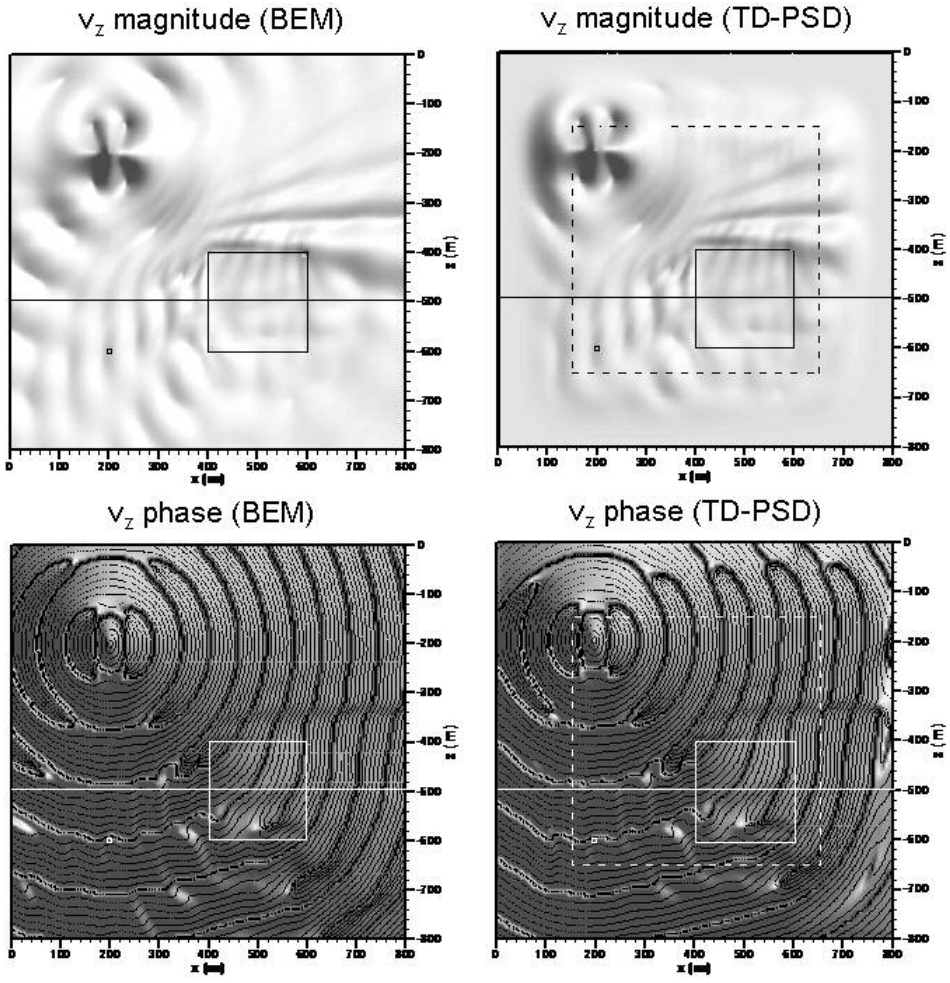
v_z magnitude (BEM)
v_z magnitude (TD-PSD)
v_z phase (BEM)
v_z phase (TD-PSD)

Figure 3

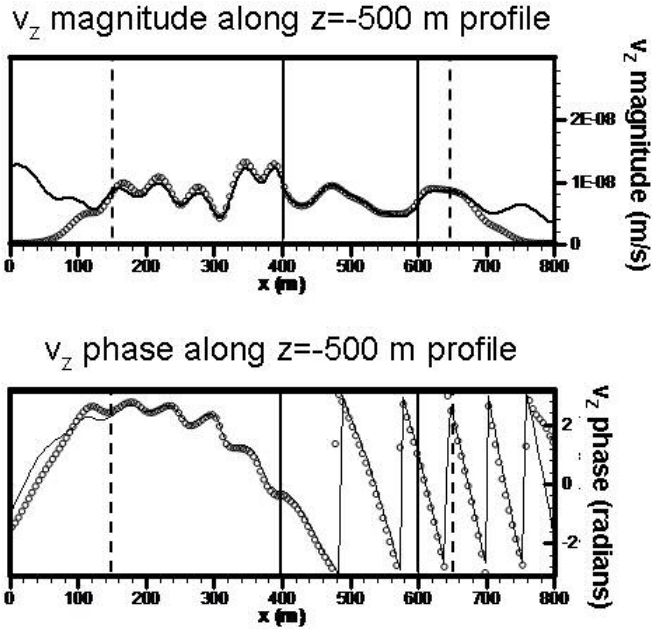
v_z magnitude along z=-500 m profile
v_z magnitude (m/s)
2E-08
1E-08
0
0
100
200
300
400
500
600
700
800
x (m)
v_z phase along z=-500 m profile
v_z phase (radians)
2
0
-2
0
100
200
300
400
500
600
700
800
x (m)

Figure 4

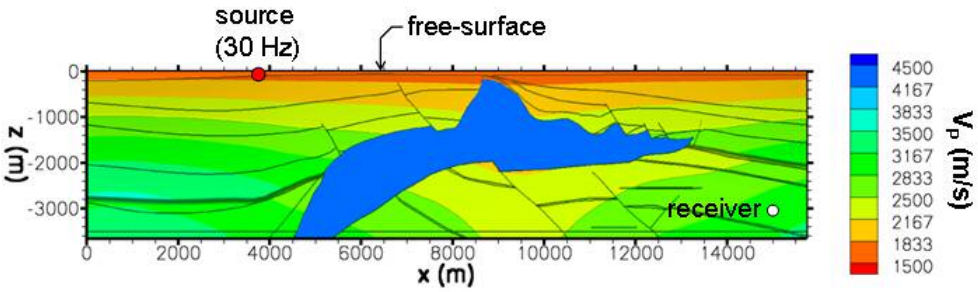
source
(30 Hz)
free-surface
receiver
z (m)
0
-1000
-2000
-3000
0
2000
4000
6000
8000
10000
12000
14000
x (m)
4500
4167
3833
3500
3167
2833
2500
2167
1833
1500
Vp (m/s)

Figure 5

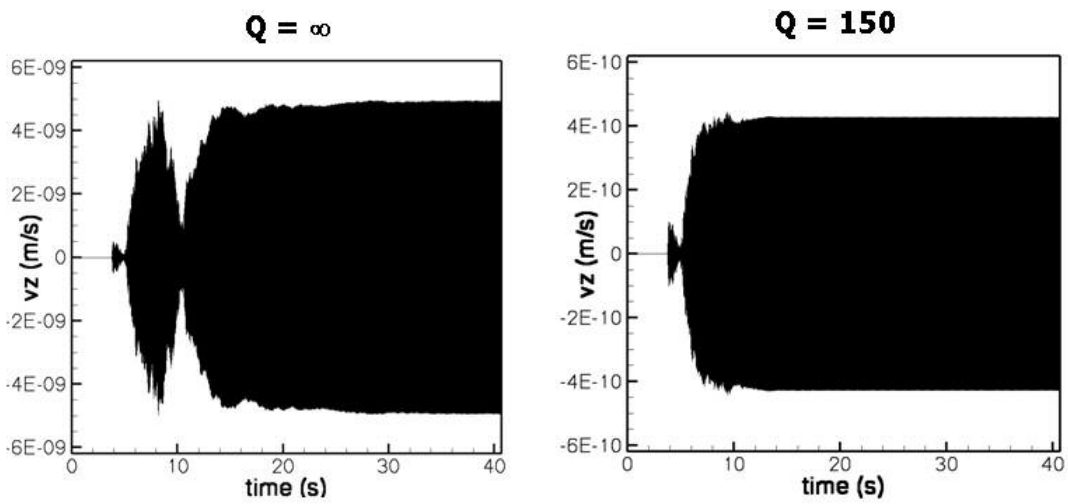
Q = ∞
6E-09
4E-09
2E-09
0
-2E-09
-4E-09
-6E-09
vz (m/s)
0
10
20
30
40
time (s)
Q = 150
6E-10
4E-10
2E-10
0
-2E-10
-4E-10
-6E-10
vz (m/s)
0
10
20
30
40
time (s)

Figure 6

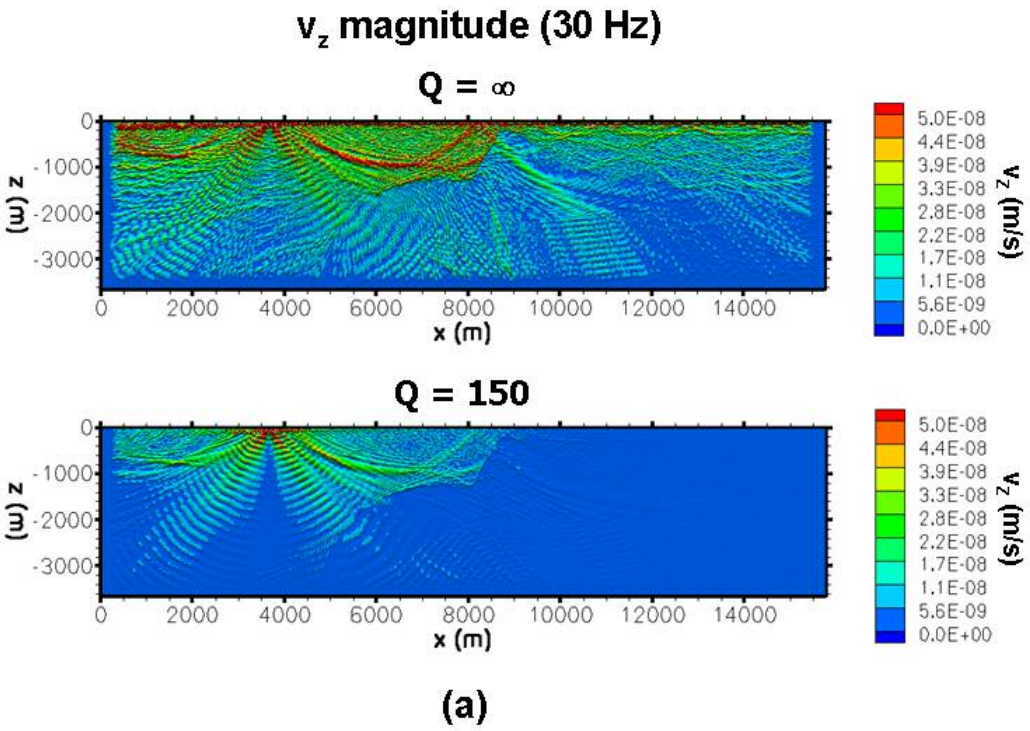
v_z magnitude (30 Hz)
Q = ∞
z (m)
0
-1000
-2000
-3000
0
2000
4000
6000
8000
10000
12000
14000
x (m)
5.0E-08
4.4E-08
3.9E-08
3.3E-08
2.8E-08
2.2E-08
1.7E-08
1.1E-08
5.6E-09
0.0E+00
v_z (m/s)
Q = 150
z (m)
0
-1000
-2000
-3000
0
2000
4000
6000
8000
10000
12000
14000
x (m)
5.0E-08
4.4E-08
3.9E-08
3.3E-08
2.8E-08
2.2E-08
1.7E-08
1.1E-08
5.6E-09
0.0E+00
v_z (m/s)
(a)

Figure 7(a)

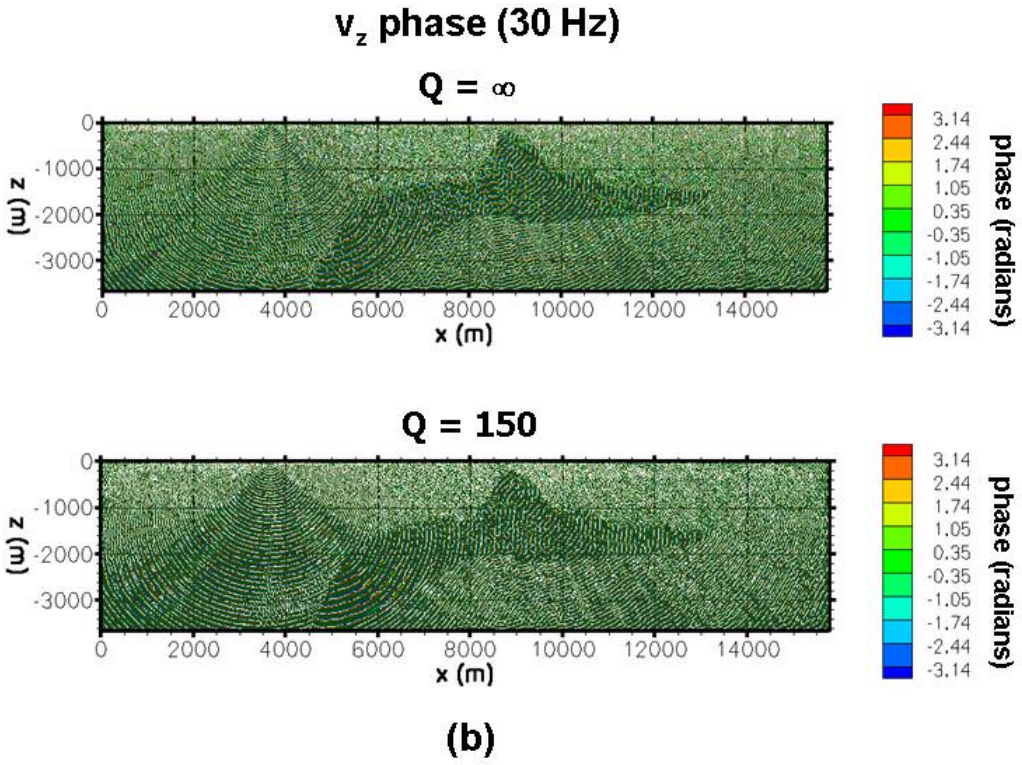
v_z phase (30 Hz)
Q = ∞
z (m)
0
-1000
-2000
-3000
0
2000
4000
6000
8000
10000
12000
14000
x (m)
3.14
2.44
1.74
1.05
0.35
-0.35
-1.05
-1.74
-2.44
-3.14
phase (radians)
Q = 150
z (m)
0
-1000
-2000
-3000
0
2000
4000
6000
8000
10000
12000
14000
x (m)
3.14
2.44
1.74
1.05
0.35
-0.35
-1.05
-1.74
-2.44
-3.14
phase (radians)
(b)

Figure 7(b)

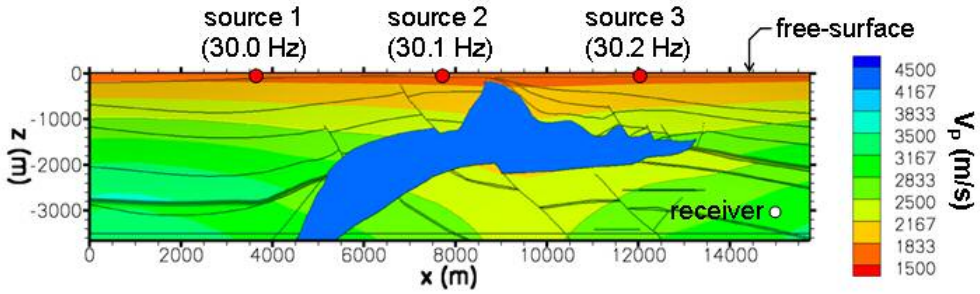
source 1
(30.0 Hz)
source 2
(30.1 Hz)
source 3
(30.2 Hz)
free-surface
receiver
z (m)
0
-1000
-2000
-3000
0
2000
4000
6000
8000
10000
12000
14000
x (m)
4500
4167
3833
3500
3167
2833
2500
2167
1833
1500
Vp (m/s)

Figure 8

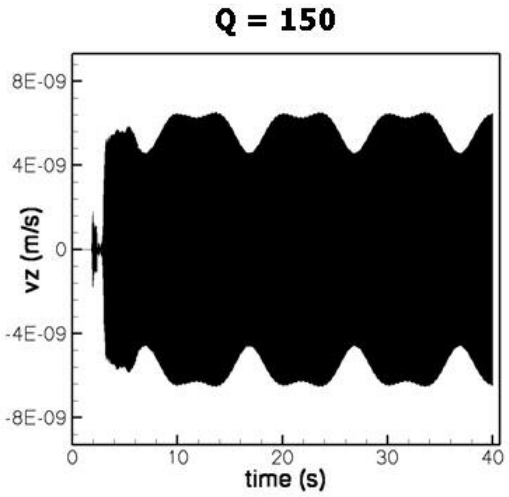

Figure 9

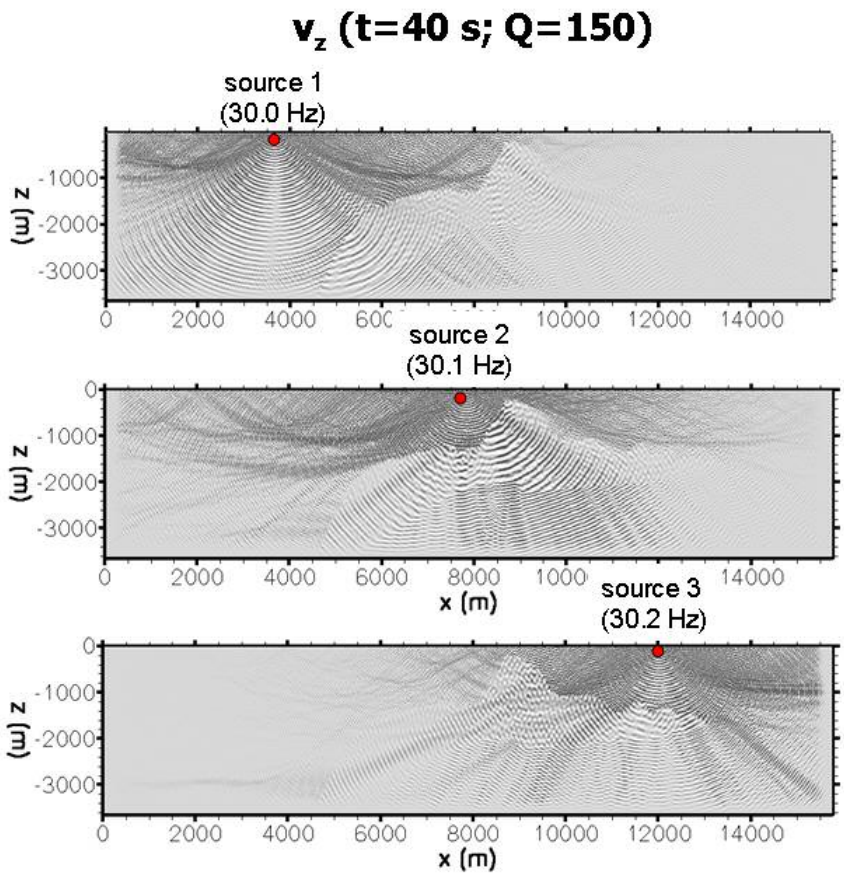
v_z (t=40 s; Q=150)
source 1
(30.0 Hz)
source 2
(30.1 Hz)
source 3
(30.2 Hz)
z (m)
x (m)
0
-1000
-2000
-3000
2000
4000
6000
8000
10000
12000
14000

Figure 10

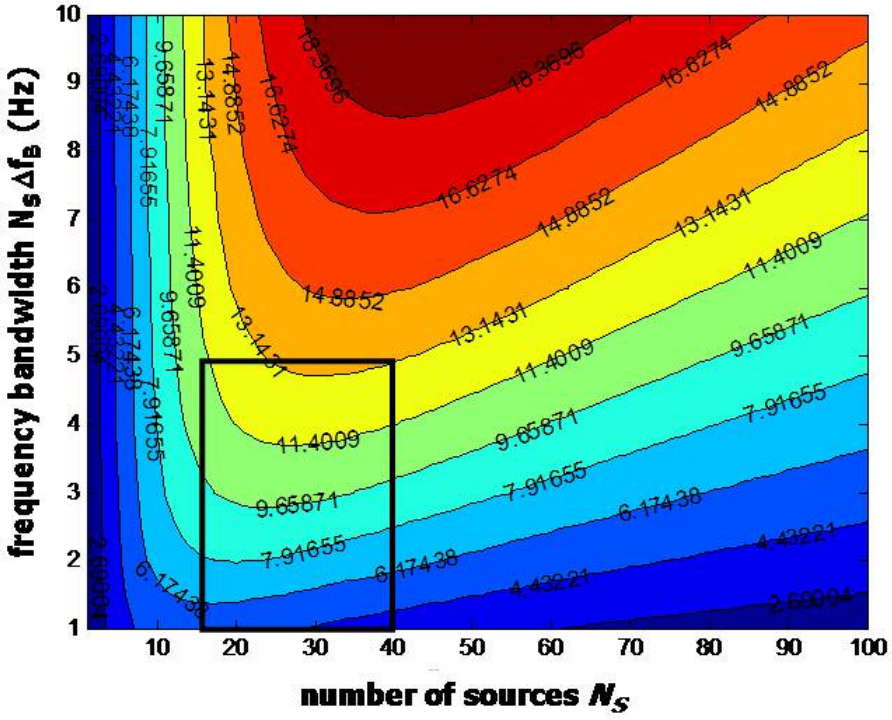
frequency bandwidth $N_s\Delta f_B$ (Hz)
number of sources N_s
10
9
8
7
6
5
4
3
2
1
10
20
30
40
50
60
70
80
90
100
18.3696
16.6274
14.8852
13.1431
11.4009
9.65871
7.91655
6.17438
4.43221
2.69004

Figure 11